

Article

Catalytic Effect of CO₂ and H₂O Molecules on •CH₃ + ³O₂ Reaction

Mohamad Akbar Ali ^{1,*} , Manas Ranjan Dash ²  and Latifah Mohammed Al Maieli ¹

¹ Department of Chemistry, College of Science, King Faisal University, Al-Ahsa 31982, Saudi Arabia; almaielilatifah@gmail.com

² Department of Chemistry, DIT University, Uttarakhand 248009, India; manas.iitm@gmail.com

* Correspondence: aamohamad@kfu.edu.sa

Abstract: The methyl (•CH₃) + ³O₂ radical is an important reaction in both atmospheric and combustion processes. We investigated potential energy surfaces for the effect of CO₂ and H₂O molecules on a •CH₃ + O₂ system. The mechanism for three reaction systems, i.e., for •CH₃ + ³O₂, •CH₃ + ³O₂ (+CO₂) and •CH₃ + ³O₂ (+H₂O), were explored using ab initio/DFT methods [CCSD(T)//M062X/6-311++G(3df,3pd)] in combination with a Rice–Ramsperger–Kassel–Marcus (RRKM)/master-equation (ME) simulation between a temperature range of 500 to 1500 K and a pressure range of 0.0001 to 10 atm. When a CO₂ and H₂O molecule is introduced in a •CH₃ + ³O₂ reaction, the reactive complexes, intermediates, transition states and post complexes become thermodynamically more favorable. The calculated rate constant for the •CH₃ + ³O₂ (3 × 10⁻¹⁵ cm³ molecule⁻¹ s⁻¹ at 1000 K) is in good agreement with the previously reported experimentally measured values (~1 × 10⁻¹⁵ cm³ molecule⁻¹ s⁻¹ at 1000 K). The rate constant for the effect of CO₂ (3 × 10⁻¹⁶ cm³ molecule⁻¹ s⁻¹ at 1000 K) and H₂O (2 × 10⁻¹⁷ cm³ molecule⁻¹ s⁻¹ at 1000 K) is at least one–two-order magnitude smaller than the free reaction (3 × 10⁻¹⁵ cm³ molecule⁻¹ s⁻¹ at 1000 K). The effect of CO₂ and H₂O on •CH₃ + ³O₂ shows non-RRKM behavior, however, the effect on •CH₃ + ³O₂ shows RRKM behavior. Our results also demonstrate that a single CO₂ and H₂O molecule has the potential to accelerate a gas-phase reaction at temperature higher than >1300 K and slow the reaction at a lower temperature. The result is unique and observed for the first time.



Citation: Ali, M.A.; Dash, M.R.; Al Maieli, L.M. Catalytic Effect of CO₂ and H₂O Molecules on •CH₃ + ³O₂ Reaction. *Catalysts* **2022**, *12*, 699. <https://doi.org/10.3390/catal12070699>

Academic Editor: Anton Naydenov

Received: 26 May 2022

Accepted: 22 June 2022

Published: 25 June 2022

Publisher's Note: MDPI stays neutral with regard to jurisdictional claims in published maps and institutional affiliations.



Copyright: © 2022 by the authors. Licensee MDPI, Basel, Switzerland. This article is an open access article distributed under the terms and conditions of the Creative Commons Attribution (CC BY) license (<https://creativecommons.org/licenses/by/4.0/>).

Keywords: •CH₃ radical; ³O₂ radical; water and CO₂ catalysis; ab initio/DFT; RRKM/ME

1. Introduction

Methyl (•CH₃) radical is the most stable intermediate species in many combustion-reaction processes [1,2]. In the Earth's atmosphere, •CH₃ radical is formed by the oxidation of methane by several tropospheric oxidizing agents such as OH, NO₃ radicals and the Cl atom. The kinetics of a •CH₃ + O₂ reaction have been a key topic in combustion chemistry for the last five decades [2–17]. The reaction mechanism behind •CH₃ oxidation is certainly an important part of the kinetic modeling of volatile organic compounds (VOCs). Several research groups have been proposed for the oxidation mechanism for the •CH₃ + O₂ reaction, as given below [2–17];



In the first reaction (R1), •CH₃ radical primarily reacts with the O₂ radical lead in the formation of formaldehyde (CH₂O) and the hydroxyl radical (OH), suggested as major products [4,8,9,11]. In the second reaction (R2), the formation of the formyl radical (HCO•) and H₂O (R2) were suggested as minor products via a hydrogen-transfer reaction followed by O–O breaking [8,9]. •CH₃ can also be oxidized to form an oxygen-centered

methoxy radical ($\bullet\text{CH}_3\text{O}$) and an O atom via O-O breaking (R3) [11]. Many experimental and theoretical studies on the $\bullet\text{CH}_3 \cdots {}^3\text{O}_2$ reaction system have been performed under atmospheric and combustion conditions [3–17]. Several research groups have used various experimental techniques, such as flash photolysis, gas chromatography, and molecular modulation spectrometry, to monitor the decay of reactants or products. By using a shock tube, the rate constants of reactions for R1 and R2 have been measured between 1000 and 3000 K [3–12]. The proposed rate constants show large discrepancies between the groups. Although vigorous experimental measurements have been carried out on the $\bullet\text{CH}_3 + {}^3\text{O}_2$ reaction, surprisingly few theoretical calculations are available in the literature [8–11]. Zhu et al. [11] performed CCSD(T)/6-3111G(3df,2p)//B3LYP/6-311G(d,p) in combination with the RRKM/master equation (ME), to compute the potential energy-surface and rate constants. Their theoretically reported rate constants for R1–R3 reactions were in good agreement with the experimentally measured values. Zhu et al. [11] also suggested that reaction R3 is insignificant in their calculations due to the high energy barrier. Very recently, Zhang et al. [8] re-visited the chemical kinetics mechanism for the $\bullet\text{CH}_3 + {}^3\text{O}_2$ reaction CCSD(T)-F12/cc-pVQZ-F12//QCISD/6-311++G(2df,2p), with RRKM/ME simulations. They reported rate constants in the temperature range from 300 to 2500 K and pressure from 0.01 to 100 atm. Their theoretically calculated rate constants were in good agreement with the recently measured values, within a factor of 2 at the temperature range of 1300–1500 K. They also used the kinetic parameters of the $\bullet\text{CH}_3 + {}^3\text{O}_2$ reaction in the methane-ignition modeling and found good agreement with the experimental measurement. However, in their calculations, a significant difference was observed at a higher temperature for reactions R2 and R3. Therefore, the estimation of rate constants should not be based on extrapolation from the experimental measurements over a limited temperature range. In this study, we have re-investigated the chemical kinetic mechanism for the formation of the most important reaction (R1), using a high-level quantum chemical method with an advanced statistical-rate theory under combustion conditions.

It is well-known that CO_2 is the most important greenhouse gas that is released into the atmosphere from fossil-fuel burning, deforestation and natural processes, such as respiration and volcanic eruptions [18]. Over the last few decades, CO_2 emissions have been increasing on a global scale, leading to global warming and acid rain [18,19]. Many efforts have been made to reduce CO_2 emissions by using carbon-capture technology and sequestration methods [18,19]. CO_2 can reach a supercritical state and is used as a diluent in many combustion chambers [18]. It is well-known that CO_2 molecules present in the atmosphere can affect many important reactions [9,17]. To understand the significance of CO_2 in the two drastically different environments, it is necessary to understand the chemical kinetics mechanism for the effect of CO_2 on the $\bullet\text{CH}_3 + {}^3\text{O}_2$ reaction. Although several studies on the oxidation reaction of the $\bullet\text{CH}_3 + {}^3\text{O}_2$ reaction are available, to the best of our knowledge only a few studies [9,17] theoretically investigated the catalytic effect of carbon dioxide (CO_2) on the $\bullet\text{CH}_3 + {}^3\text{O}_2$ and $\text{HO} + \text{CO}$ reaction systems [9,17]. Masunov et al. [9] have investigated the mechanism for the $\bullet\text{CH}_3 + {}^3\text{O}_2$ reaction with and without the presence of CO_2 , using M11/6-311G** + GD3. They have found that the formation of a van der Waals (vdW) complex stabilized the transition states (TSs), which lowered the barrier heights. Based on thermodynamics data, they proposed that the effect of CO_2 is significant under combustion conditions. They also suggested that the chemical kinetic analysis for the effect of CO_2 on $\text{CH}_3 + \text{O}_2$ reaction is underway. Therefore, in this study, we have re-investigated the effect of CO_2 on the $\bullet\text{CH}_3 + {}^3\text{O}_2$ reaction using a similar level of theory in combination with an advanced statistical-rate theory, to understand the chemical kinetic behavior for the effect of CO_2 on $\bullet\text{CH}_3 + {}^3\text{O}_2$.

Over the last few years, numerous investigations have been made into the catalytic effect of a single H_2O molecule on many atmospheric and combustion reaction systems, such as $\text{CH}_3\text{OH} + \text{OH}$, $\text{HCHO} + \text{OH}$, $\text{C}_2\text{H}_4 + \text{OH}$, $\text{CH}_3\text{CHO} + \text{OH}$, $\text{CH}_3\text{C}(=\text{O})$, $\text{CH}_3\text{C}(=\text{O})\text{CH}_3 + \text{OH}$ and $\text{CH}_2\text{NH} + \text{OH}$ as well as $\text{CH}_3\text{O} + \text{O}_2$, $\text{OH} + \text{CH}_4$, $\text{CH}_2\text{OH} + \text{O}_2$ and $\text{H}_2\text{O}_2 + \text{OH}$ reactions [20–36]. All of these studies indicate that a single H_2O molecule

makes complexes, transition states and post complexes thermodynamically more stable than a water free-reaction, due to the formation of more hydrogen-bonded species. The above studies suggested that the reaction-rate constant decreases due to the presence of a high water concentration. In our recent works, we proposed the catalytic effect of H₂O molecule on the $\bullet\text{CH}_2\text{OH} + \text{O}_2$ reaction system and suggested that the catalytic role of water is insignificant under atmospheric and combustion conditions [26]. The calculated rate constant for the $\bullet\text{CH}_2\text{OH} + {}^3\text{O}_2$ reaction at room temperature (298 K) is in good agreement with the previously measured values at the same level of theories. We suggested that when H₂O molecule is added to the reaction, the formation of CH₂O and HO₂ is dominated under higher temperature conditions.

There are no theoretical chemical kinetic details for the catalytic effect of the CO₂ and H₂O molecules on the $\bullet\text{CH}_3 + {}^3\text{O}_2$ reaction in the gas phase. In this work, for the first time, we have investigated the rate constants for the effect of CO₂ and H₂O molecules on the most important atmospheric and combustion prototype reactions, i.e., $\bullet\text{CH}_3 + {}^3\text{O}_2$. The temperature and pressure-dependent rate constants are computed in the temperature range between 500 and 1500 K and 0.0001 to 10 atm, using the RRKM/ME simulation for all three reaction systems. To assess the accuracy of our results, we have compared the energies and rate constants for the $\bullet\text{CH}_3 + {}^3\text{O}_2$ and $\bullet\text{CH}_3 + {}^3\text{O}_2 + (\text{CO}_2)$ reaction systems with the available literature values. We hope this study is potentially important to design and analyze the possible forms of nonpetroleum-based fuel or fuel components in combustion engines.

2. Computational Methodology

2.1. Electronic-Structure Calculations

All the quantum chemical calculations were carried out with the Gaussian 09 suite of programs [37]. All the species involved in the $\bullet\text{CH}_3 + \text{O}_2$, $\bullet\text{CH}_3 + {}^3\text{O}_2 (+\text{CO}_2)$ and $\bullet\text{CH}_3 + \text{O}_2 (+\text{H}_2\text{O})$ reactions were optimized using the hybrid-density functional theory, i.e., M062X [designated as [M0] [38]] with Pople basis set 6-311++G(3df,3pd) [designated as [p] (see Table S1)]. We have used a reasonably high polarized and diffuse function of the Pople basis set 6-311++G(3df,3pd), which is reasonably good for the system studies here. We have used 6-311++G(3df,3pd) for a similar system in our earlier calculations [26–28], which has been used by many other researchers for the rate constants' calculation. To add the correction from the van der Waal interaction on M0-p, the Grimme empirical dispersion correction "GD3", was used. The vibrational frequency of each species was calculated to estimate the zero-point corrections (ZPE) and the vibrational partition functions and density of the states. All the optimized structures have real vibrational frequency except the transition states, which have one imaginary mode (see the Table S2). The vibrational mode, which corresponds to the Hindered Rotor (HR), was treated as HR approximation in the densum-input file. To further improve the accuracy of energy, the single-point energy calculations were performed at CCSD(T)/6-311++G(3df,3pd) [designated CC-p] level [28–33]. The RCCSD(T) method was used for closed-shell species, such as CH₂O and H₂O, CO₂, and for all open-shell species the UCCSD(T) method was used. The combination of CC-p and M0-p generally gives the result that is accurate of $\sim 1 \text{ kcal mol}^{-1}$, which is $\sim 20\%$ error in the computed rate constant at 1000 K. Several research groups have already used M0-p with CC-p to calculate the energies and rate constants. The results reported by them were in good agreement with the experimentally measured values [28,30]. The entrance channels for the addition reactions have no intrinsic energy barriers. For a better description of the wave function "GUESS=MIX" keyword was used for the addition reactions. The "GUESS=MIX" option mixes the HOMO and LUMO orbitals to break spatial symmetry. The "GUESS=MIX" option was only used for geometry optimization.

2.2. Chemical Kinetics Calculations

For pressure-dependent reactions, the energy-dependent specific unimolecular rate constant $k(E)$ was calculated using RRKM statistical rate theory given by [39] Equation (1):

$$k(E) = L \neq \frac{1}{h} \frac{G^\ddagger(E - E_0)}{\rho(E)} \quad (1)$$

The details of each term in the Equation (1) are given in the Chemical Kinetics Section of Supporting Information and MultiWell user manual [39].

At each temperature and pressure, master equation simulations were initiated using the chemical-activation energy distribution, which is appropriate for recombination reactions [39]. The pressure-dependent total rate constants $k^{bimol}(T, M)$ for $\bullet\text{CH}_3 + \text{O}_2$, $\bullet\text{CH}_3 + \text{O}_2 (+\text{CO}_2)$ and $\bullet\text{CH}_3 + \text{O}_2 (+\text{H}_2\text{O})$ were calculated using [39] Equation (2):

$$k^{bimol}(T, M) = K_{eq} \times k_{\infty}^{uni} (1 - f_R) \quad (2)$$

The MultiWell code was used to calculate the branching fraction (f) for each reaction and calculate the unimolecular rate constants (k_{uni}). The pressure-dependent rate constants were simulated using estimated energy-transfer parameters for the complexes and intermediates. The tunnelling corrections were implemented based on asymmetric Eckart potential. The approximated temperature-dependent exponential down $\langle \Delta E \rangle_{\text{down}} = 200 * (T/300)^{0.85} \text{ cm}^{-1}$ [28,32] was used to calculate the rate constants. The details about the energy-grain parameter to calculate the rate constant are given in the chemical kinetic section of the Supporting Information.

The equilibrium constant (K_{eq}) for the formation of the complexes was calculated using THERMO code as given in Equation (3):

$$K_{eq} = \frac{Q_{\text{Complex}}}{Q_{\text{reactants}}} \exp\left(-\frac{E_{\text{complex}} - E_{\text{reactants}}}{k_B T}\right). \quad (3)$$

The equilibrium constant values were tabulated in Supporting Information Table S3.

3. Results and Discussion

3.1. Reaction Pathways for $\bullet\text{CH}_3 + {}^3\text{O}_2$

Figure 1 shows the zero-point corrected PES for the $\bullet\text{CH}_3 + {}^3\text{O}_2$ reaction and the energies of reactants, pre-reactive complex (RC), intermediates (Ints), transition states (TSs), post complexes (PCs) and products are tabulated in Table 1. The optimized geometries of reactants, RCs, Ints, PCs, TSs and products are given in Supporting Information Table S1. In the $\bullet\text{CH}_3$ radical, an unpaired electron resides on the carbon atom. When O_2 molecule attacks the carbon atom of $\bullet\text{CH}_3$, the new C–O bond leads to the formation of an intermediate $\bullet\text{OO-CH}_3$ (Int-1). The pathway is shown using a red dashed line in Figure 1. Recently, Masunov et al. [9] proposed a mechanism for the formation of the reactive complex (RC) with ~ 1 kcal/mol energy, followed by a transition state TS1 leading to form Int-1. We have also optimized the RC and TS1 using the M0-p method, and our results are very similar to Masunov et al.'s values [9]. The computed stabilization energy of Int-1 (RO_2) is $-29.3 \text{ kcal mol}^{-1}$, which is in very good agreement with the previously reported values [8,9]. In the RO_2 (Int-1), the adduct can further rearrange to form QOOH (Int-2) via 1–3 hydrogen shift TS2 with $+15.9 \text{ kcal mol}^{-1}$, with respect to the reactants. The barrier height for this pathway is $\sim 45 \text{ kcal mol}^{-1}$ (relative to Int-1), which is in very good agreement with the previous studies. As discussed in the earlier studies, this step is the rate-determining step of the reaction and is most favored in the high-temperature range. The stabilization energy of Int-2 is calculated to be $-16.7 \text{ kcal mol}^{-1}$, which can further dissociate via a barrierless-transition state TS3 ($-19.0 \text{ kcal mol}^{-1}$). The stabilization of this TS is due to the formation of a five-membered hydrogen-bonded complex (PC). The calculated energy for Int-3 is $-55.8 \text{ kcal mol}^{-1}$, which subsequently leads to the formation

of OH and CH₂O. The calculated energies for TS1, TS2, Int-2, TS3, PC and HO + CH₂O are also in good agreement with the previously reported values [9,11]. It is important to mention how the H-bonding interaction affects the energies of the TS and complexes. In the PC, the hydrogen bond is formed between the H-atom of the OH radical and the O-atom of the CH₂O, whereas Int-1 and Int-2 are non-hydrogen bonded moieties. Therefore, the PC is the most stable among all these species.

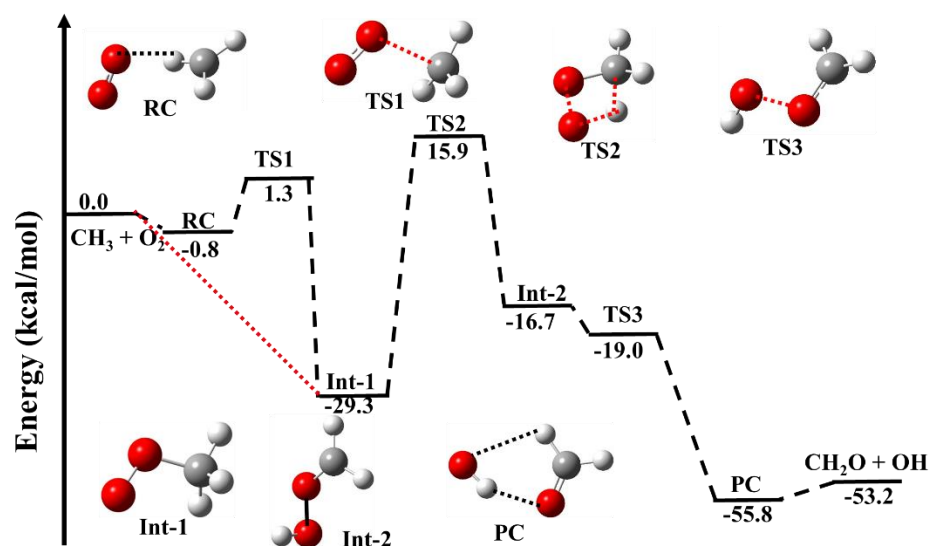


Figure 1. Zero-point corrected potential energy surface for $\bullet\text{CH}_3 + {}^3\text{O}_2$ reaction calculated using CC-p//M0-p level. The red-dashed-line pathway is based on earlier studies.

Table 1. Enthalpies of reaction (ΔH_{rxn} (0 K) in kcal mol⁻¹ for $\bullet\text{CH}_3 + \text{O}_2$ reaction.

$\bullet\text{CH}_3 + \text{O}_2 \rightarrow$	This Work	Literature
OO...CH ₃ (RC)	-0.8	-0.4 ^b
OO...CH ₃ (TS1)	1.3	1.6 ^b
CH ₃ OO (Int-1)	-29.3	-30.4 ^a , -33.8 ^b
HOO...CH ₂ (TS2)	+15.9	15.0 ^a , 13.7 ^b
HO...CH ₂ O (Int-2)	-16.7	-18.5 ^a , -20.6 ^b
HO...CH ₂ O (TS ₃)	-19.0	-21.3 ^b
HO...CH ₂ O (PC)	-55.8	-58.2 ^b
CH ₂ O + OH	-53.2	-53.7, -52.10 ^c
$\bullet\text{CH}_3 + \text{O}_2 + \text{CO}_2 \rightarrow$		
CH ₃ ...O ₂ + CO ₂	-0.8	-0.4 ^b
CO ₂ ...CH ₃ OO (RC-c)	-2.5	-2.6 ^b
CO ₂ ...CH ₃ OO (TS1-c)	3.3	-0.3 ^b
CO ₂ ...CH ₃ OO (Int-1c)	-31.0	-37.0 ^b
CO ₂ ...CH ₃ OO (TS2-c)	13.0	8.7 ^b
CO ₂ ...CH ₃ OO (Int-2c)	-19.5	-25.0 ^b
CO ₂ ...CH ₃ OO (TS-3c)	-22.0	-25.4 ^b
HO...CH ₂ O...CO ₂ (PC-c)	-56.9	-61.6 ^b
$\bullet\text{CH}_3 + \text{O}_2 + \text{H}_2\text{O} \rightarrow$		
CH ₃ ...O ₂ + H ₂ O	-0.8	
H ₂ O...CH ₃ OO (RC-h)	-4.8	
H ₂ O...CH ₃ OO (TS1-h)	0.3	
H ₂ O...CH ₃ OO (Int-1h)	-32.5	
H ₂ O...CH ₃ OO (TS2-h)	13.6	
H ₂ O...CH ₃ OO (Int-2h)	-21.7	
H ₂ O...CH ₃ OO (TS3-h)	13.6	
HO...CH ₂ O...H ₂ O (PC-h)	-61.7	

^a Zhu et al. [11], ^b Masunov et al. [9] and ^c ATcT thermochemical data [40–42].

Our calculated reaction energies for $\bullet\text{CH}_3 + {}^3\text{O}_2 \rightarrow \text{CH}_2\text{O} + \text{OH}$ are also in good agreement (-53.7 kcal/mol) with the most recent release thermochemical value (-52.1 kcal/mol) [40–42]. The literature's thermochemical values (ATcT) are a new paradigm of how to develop the most accurate thermochemical data given by Argonne National Lab, Lemont, Illinois, USA [40–42]. As discussed in the previous section, the most important channel in the combustion condition for the $\bullet\text{CH}_3 + {}^3\text{O}_2$ reaction is leading to form the CH_2O , so we focused only on the R1 channel in the current study, and the energies of other pathways are neglected. To avoid any repetition, we have restricted our discussion to only reaction R1, as related discussion to the R2 and R3 channels can be found in the literature [9,11].

3.1.1. Reaction Pathways for $\bullet\text{CH}_3 + {}^3\text{O}_2 (+\text{CO}_2)$

Figure 2 shows the PES for the CO_2 -catalyzed $\bullet\text{CH}_3 + {}^3\text{O}_2$ reaction, and the energies are tabulated in Table 1. The optimized parameters of RC-c, Ints-c, TSs-c and PC-c are given in Table S1. As suggested in the previous work [20–37], the possibilities of molecular collisions between O_2 , $\bullet\text{CH}_3$ and CO_2 are very unlikely, therefore, we believe that $\bullet\text{CH}_3$ and O_2 collide first to form an RC complex, and this complex collides with CO_2 to form a three-molecular complex, i.e., RC-c. Based on our previous knowledge and the previous studies, we believe that the RC is more important (negative energy) than $\text{CH}_3\cdots\text{CO}_2$ and $\bullet\text{CO}_2\cdots\text{O}_2$ (positive energy). Therefore, the complexes $\bullet\text{CH}_3\cdots\text{CO}_2$ and $\text{CO}_2\cdots\text{O}_2$ are not considered in PES profile. As discussed in the earlier study [9], the CO_2 -catalyzed reaction proceeds via similar reaction channels as the uncatalyzed pathways, but the reaction mechanism becomes quite different, resulting in different energies than the uncatalyzed species. For more simplicity, we have used only the minimum energy structure in the current study. As shown in Figure 2, the binding energy of RC is -0.8 kcal mol $^{-1}$ combined with CO_2 , leading to form a $\text{CO}_2\cdots\text{CH}_3\cdots\text{O}_2$ (RC-c) with stabilization energy of -2.5 kcal mol $^{-1}$. This value is in good agreement with previously reported values [9] (Table 1). The RC-c can further proceed by binding the diatomic oxygen to the methyl group, to form an intermediate $\text{CO}_2\cdots\text{CH}_3\text{OO}$ (Int-1c) via TS1-c. The calculated barrier height (~ 6 kcal/mol) is ~ 4 kcal/mol higher than the uncatalyzed reaction. Therefore, we can say that CO_2 does not act as a catalyst for this pathway. It is also important to mention that CO_2 acts as a catalyst for RC-c and Int-1c. This result is due to the formation of a hydrogen bond between the H-atom of CH_3O_2 and O-atom CO_2 (2.6 Å). The Int-1c can further transfer to the Int-2c via an intramolecular hydrogen-atom transfer from the terminal oxygen of CH_3OO via a four-membered cyclic-transition state with a high energy barrier. The barrier height (44 kcal/mol) for this pathway is 2 kcal/mol lower than the uncatalyzed pathway. In this pathway, the CO_2 acting as a catalyst reduces the energy barrier by 2 kcal/mol. The intermediate Int-2c can further transfer to PC-c with a barrierless transition state TS3-c, which can dissociate into $\text{CH}_2\text{O} + \text{OH} + \text{CO}_2$.

The stabilization energy of Int-2c and PC-c are lower than the corresponding uncatalyzed structures (see Table 1). This can be also explained by the formation of hydrogen bonds. Int-2 (Figure 1) is a non-hydrogen-bonded structure, whereas the corresponding CO_2 -catalyzed analog Int-2c formed a strong hydrogen-bonded complex between the H-atom of OH and the O-atom of CO_2 (2.1 Å). On the other hand, PC-c formed a seven-membered ring-like structure with two strong hydrogen bonds, between the terminal H-atom of CH_2O and the O-atom of OH (2.5 Å) as well as the H-atom of OH and the O-atom of CO_2 (2.0 Å), compared to the less stable five-membered ring-like structure with two hydrogen bonds in the uncatalyzed analog (PC). Similarly, TS3-c (-22.0 kcal mol $^{-1}$) is more stable than the corresponding uncatalyzed-transition state (TS3), due to the hydrogen-bonding interaction. In general, the RC-c, TSs-c, Ints-c and PC-c are thermodynamically more favorable by 2 kcal/mol than the RC, TSs, Ints and PC species. The calculated energies of all the CO_2 -catalyzed structures are in good agreement with the recently reported values (see Table 1) [9].

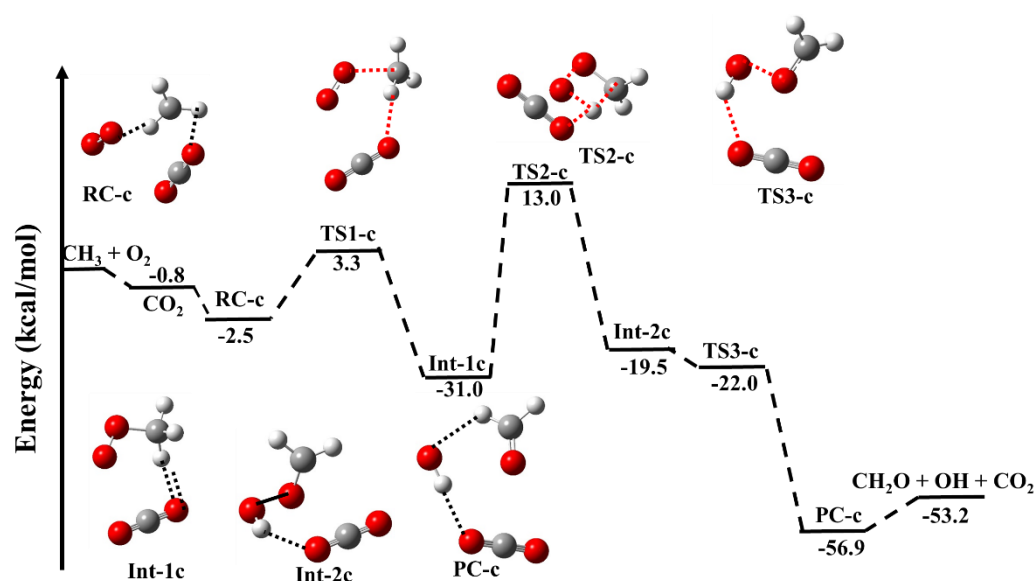


Figure 2. Zero-point corrected potential energy surface for $\bullet\text{CH}_3 + \text{O}_2$ ($+\text{CO}_2$) reaction calculated using CC-p//M0-p level.

3.1.2. Reaction Pathways for $\bullet\text{CH}_3 + {}^3\text{O}_2$ ($+\text{H}_2\text{O}$)

Figure 3 shows the zero-point corrected PES for the effect of H_2O on the $\bullet\text{CH}_3 + {}^3\text{O}_2$ reaction. The energies for effect of H_2O on complex (RC-h), intermediates (Ints-h), TSs-h and PC-h are tabulated in Table 1. The geometrical parameters for all the species are tabulated in Supporting Information Tables S1 and S2. The effect of H_2O on the $\bullet\text{CH}_3 + {}^3\text{O}_2$ reaction proceeds via similar reaction channels, as discussed in the CO_2 -catalyzed reaction with different reaction energies. As mentioned earlier, the three molecular collisions are very uncommon. Therefore, we believe the RC formed first, which collides with H_2O to form $\text{H}_2\text{O}\cdots\text{CH}_3\cdots\text{O}_2$ (RC-h) with a stabilization energy of $-4.8 \text{ kcal mol}^{-1}$. This value is nearly 2 kcal/mol lower than the CO_2 -catalyzed reaction and 4 kcal/mol lower than the uncatalyzed reaction. This is due to the formation of a higher number of H-bonds in the RC-h. The RC-h can further proceed via TS1-h to form $\text{H}_2\text{O}\cdots\text{CH}_3\text{OO}$ (Int1-h). It is important to notice that the effect of H_2O lowers the stabilization energy of Int-1h by 3 kcal mol^{-1} , however, the effect of CO_2 lowered the energy by $\sim 1.5 \text{ kcal mol}^{-1}$ compared to the uncatalyzed pathway. The result suggests the catalytic behavior of H_2O is more significant than CO_2 . This is due to the formation of a strong hydrogen bond between the H atom of CH_3O_2 and the O atom of H_2O (2.0 \AA), in comparison with the formation of a weaker hydrogen bond (2.6 \AA) in the case of CO_2 . Similarly, the barrier height of the H_2O -catalyzed transition state (TS1-h) is 3 kcal mol^{-1} more stable than the CO_2 -catalyzed transition state (TS1-c); this difference can be seen by the formation of two hydrogen bonds in TS1-h between the O-atom of O_2 and the H-atom of H_2O (2.2 \AA) as well as the O-atom of H_2O and the H-atom of CH_3 (2.6 \AA), whereas, in the case of TS1-c, only one hydrogen bond is formed between the O-atom of CO_2 and the H-atom of CH_3 (3.0 \AA). A hydrogen atom is transferred intramolecularly from Int-1c via a four-membered cyclic-transition state, TS2-h, with high energy. The barrier height of TS2-h is $\sim 46 \text{ kcal/mol}$ is higher than the barrier height of a similar transition state of a CO_2 -catalyzed species, i.e., TS2-c ($\sim 44 \text{ kcal/mol}$). It has been observed that the stabilization energies of H_2O -catalyzed species, i.e., Int2-h and PC-h, are lower than the corresponding CO_2 -assisted reaction. These results are due to the formation of a stronger H-bond in the water environment than a weak interaction in the CO_2 environment. In general, the reaction species in the presence of a H_2O is thermodynamically more favorable by $3\text{--}5 \text{ kcal/mol}$ than the uncatalyzed reaction and $\sim 2 \text{ kcal/mol}$ more favorable than the CO_2 -assisted reaction. The result of the water effect on the $\text{CH}_3 + \text{O}_2$ reaction is unique and has not been published in the literature.

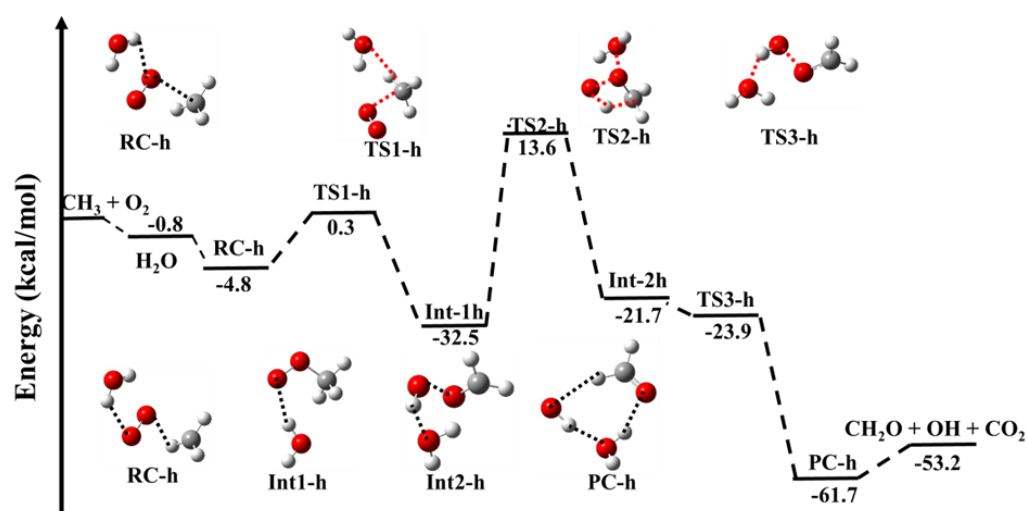


Figure 3. Zero-point corrected potential energy surface for $\cdot\text{CH}_3 + \text{O}_2 (+\text{H}_2\text{O})$ calculated using CC-p//M0-p level.

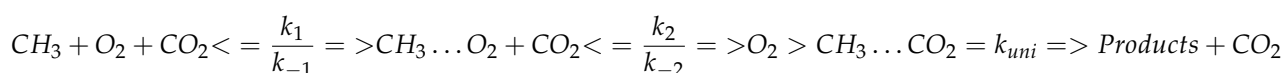
3.2. Rate Constants

3.2.1. $\cdot\text{CH}_3 + {}^3\text{O}_2$ Reaction

Figure 4 shows the rate constants for the $\cdot\text{CH}_3 + {}^3\text{O}_2$ reaction obtained using the CC-p//M0-p method coupled with RRKM/ME simulations in the temperature range of 500–1500 K under a high pressure limit. The $\cdot\text{O}_2\text{-CH}_3$ that is assumed to play important roles in the $\cdot\text{CH}_3 + {}^3\text{O}_2$ reaction system is formed via the entrance channel, which has a well depth of ~ 30 kcal/mol. The rate constants for the formation of $\cdot\text{O}_2\text{-CH}_3$ are pressure-dependent and negative-temperature dependent. This result is consistent with previously reported ones [8,11]. The rate constants are also calculated for the new reaction mechanism, i.e., $\text{R} \rightarrow \text{RC} \rightarrow \text{Int-1} \rightarrow \text{Int-2} \rightarrow \text{PC} \rightarrow \text{CH}_2\text{O} + \text{OH}$, as shown in Figure 1. In this case, we have observed that the reaction is independent of pressure, and the rate constant is at least two-order magnitude smaller than the $\text{R} \rightarrow \text{Int-1} \rightarrow \text{Int-2} \rightarrow \text{PC} \rightarrow \text{CH}_2\text{O} + \text{OH}$ channel. The proposed mechanism, based on Masunov et al. [9], is inconsistent with the previously reported rate constants [9]. Therefore, we believe that the mechanism via Int-1 is the most appropriate way to deal with the combustion-reaction system. Therefore, the formation of RC should be neglected from the $\cdot\text{CH}_3 + {}^3\text{O}_2$ reaction channel. The formation of RC may not even be important in the atmospheric condition due to its short lifetime. The calculated rate constants are also compared with some of the previous studies, as shown in Figure 4. Our values are in good agreement with the value of Zhang et al. [8] at higher temperature. We have observed that the formation of $\text{CH}_2\text{O} + \text{OH}$ is almost negligible (< 1300 K), which is also consistent with Zhang et al. [8] and Zhu et al. [11]. Due to the large number of data available for the $\cdot\text{CH}_3 + {}^3\text{O}_2$ reaction, we restrict our discussion to only a few of the literature values to avoid repetition, plus the main focus of the current study is to compare the results of the catalytic effect of CO_2 and H_2O on the $\cdot\text{CH}_3 + {}^3\text{O}_2$ reaction.

3.2.2. Effect of CO_2 on $\cdot\text{CH}_3 + {}^3\text{O}_2$ Reaction

The scheme for the formation of CH_2O and OH from the $\cdot\text{CH}_3 + \text{O}_2$ reactions in the presence of a CO_2 catalyst can be expressed as:



The high-pressure limit-rate constant was calculated using Equation (2), and the $K_{eq} = \frac{k_2}{k_{-2}}$ are the equilibrium constants of each reaction pathway involved in the $\cdot\text{CH}_3 + \text{O}_2$ reaction. The rate constants for $\cdot\text{CH}_3 + {}^3\text{O}_2 (+\text{CO}_2)$ in the temperature range of 500 to 1500 K

are tabulated in Table 2 and shown in Figure 5. Our results show that the rate constants, without including the concentration of CO₂, are higher than the $\bullet\text{CH}_3 + {}^3\text{O}_2$ reaction in the temperature range of 500 to 1500 K. In general, the rate constants of the CO₂-catalyzed reaction are higher than the $\bullet\text{CH}_3 + {}^3\text{O}_2$ reaction in the entire temperature range (see Figure 5). As discussed in our previous studies [26–32] under pseudo-first-order conditions, the relative equilibrium concentrations strongly depend on the concentration of the excess CO₂, and the correct equation to calculate the effective rate constant is $k_c^{eff} = K_{eq(1)} \times k(RRKM) \times [\text{CO}_2]$. The concentration of CO₂ diluent was converted from the pressure and temperature using real-gas behavior, as tabulated in the NIST database [43], which is based on Masunov et al.'s study analysis [9]. Masunov et al. [9] suggested that the $\bullet\text{CH}_3 + {}^3\text{O}_2$ reactions are catalyzed by CO₂, based on the analysis of PES. They suggested that the details of the chemical kinetics mechanism and a comparison with the experimental verification and improvement of the chemical kinetic details are underway [9,44]. Due to the missing information of the rate constants for the effect of CO₂ on the $\bullet\text{CH}_3 + {}^3\text{O}_2$ reaction, we have investigated the effect of CO₂ on $\bullet\text{CH}_3 + {}^3\text{O}_2$, and the rate constants' details are given in Table 2 and shown in Figure 5.

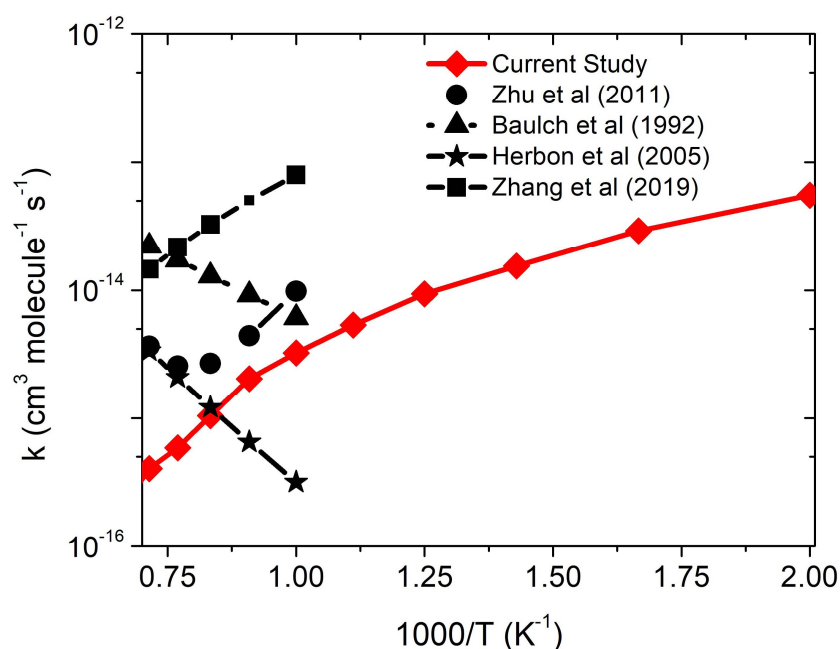


Figure 4. Rate constants for $\bullet\text{CH}_3 + {}^3\text{O}_2$ reaction in the temperature range of 500–1500 K [3,5,8,11].

Table 2. Calculated rate constants for $\bullet\text{CH}_3 + \text{O}_2$, $\bullet\text{CH}_3 + \text{O}_2 + (\text{CO}_2)$ and $\bullet\text{CH}_3 + \text{O}_2 + (\text{H}_2\text{O})$ in the temperature range of 500 to 1500 K.

Temp	$k_{\text{CH}_3+\text{O}_2}$	k_c^{eff}	k_h^{eff}
500	5.5×10^{-14}	7.6×10^{-17}	1.7×10^{-19}
600	2.9×10^{-14}	9.6×10^{-17}	6.4×10^{-19}
700	1.5×10^{-14}	1.3×10^{-16}	1.8×10^{-18}
800	9.4×10^{-15}	1.7×10^{-16}	4.5×10^{-18}
900	5.3×10^{-15}	2.3×10^{-16}	9.5×10^{-18}
1000	3.2×10^{-15}	3.0×10^{-16}	1.8×10^{-17}
1100	2.1×10^{-15}	3.9×10^{-16}	3.4×10^{-17}
1200	1.0×10^{-15}	5.04×10^{-16}	5.8×10^{-17}
1300	5.9×10^{-16}	6.41×10^{-16}	9.5×10^{-17}
1400	4.0×10^{-16}	8.2×10^{-16}	1.5×10^{-16}
1500	2.1×10^{-16}	1.02×10^{-15}	2.3×10^{-16}
$k = AT^n \exp(-B/T)$	$A = 2.8 \times 10^{14}$ $n = -9.1$ $B = 3516$	$A = 2.5 \times 10^{-33}$ $n = 4.4$ $B = -1711$	$A = 3.3 \times 10^{-33}$ $n = 5.4$ $B = 1338$

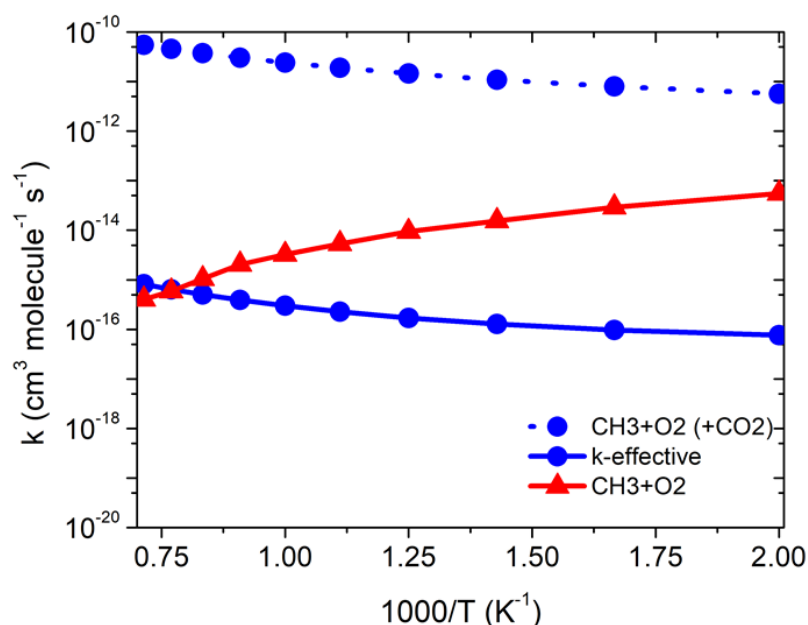
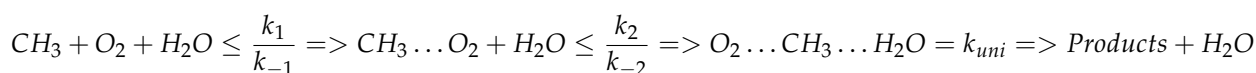


Figure 5. Rate constants for the effect of CO₂ on $\bullet\text{CH}_3 + {}^3\text{O}_2$ reaction in the temperature range of 500–1500 K.

As expected, the effective rate constants are two-order magnitude smaller at temperature < 1000 K, with a one-order-magnitude difference between 1000–1200 K. The effective rate constants suggest that the catalytic effect may be pronounced at a high temperature > 1400 K, due to a high entropic factor. The new chemical kinetics results might help to understand and design the experimental measurement. Our chemical kinetics analysis also suggests that the catalytic effect of CO₂ is dominated at higher temperature (>1400 K), which is consistent with the result of Masunov et al. [9], who suggested that the catalytic effect of CO₂ may be important at >1000 K. It is interesting to mention that the formation CH₂O is unfavorable in the RRKM/ME simulation, and the calculated rate constants are independent of the pressure, therefore, we can say that the effect of CO₂ on the CH₃ + O₂ reaction shows a non-RRKM behavior, which can be treated using a simple canonical transition state method. However, the result reported in the current study in the high-pressure limit condition can be similar to a CTST method.

3.2.3. Effect of H₂O on $\bullet\text{CH}_3 + {}^3\text{O}_2$ Reaction

The formation of CH₂O and OH from $\bullet\text{CH}_3 + {}^3\text{O}_2$ reactions in the presence of H₂O can be expressed as:



The bimolecular-rate constant can be calculated as given in Equation (2). The equilibrium constant $K_{eq(1)} = \frac{k_1}{k_{-1}}$ and the $K_{eq} = \frac{k_2}{k_{-2}}$ constants of each reaction pathway involved in the $\bullet\text{CH}_3 + \text{O}_2$ reaction were calculated and given in Supporting Information Table S3. Figure 6 shows the rate constants for $\bullet\text{CH}_3 + {}^3\text{O}_2$ (+H₂O), calculated in the temperature range of 500 to 1500 K. The rate constant for the RC + H₂O reaction ($6 \times 10^{-9} \text{ cm}^3 \text{ molecule}^{-1} \text{ s}^{-1}$ at 1000 K) is ~six-order magnitude higher than the $\bullet\text{CH}_3 + \text{O}_2$ reaction ($3 \times 10^{-15} \text{ cm}^3 \text{ molecule}^{-1} \text{ s}^{-1}$ at 1000 K). The rate constants for the effect of water are higher than the CH₃ + O₂ reaction in the entire temperature range of 500–1500 K (see Figure 6).

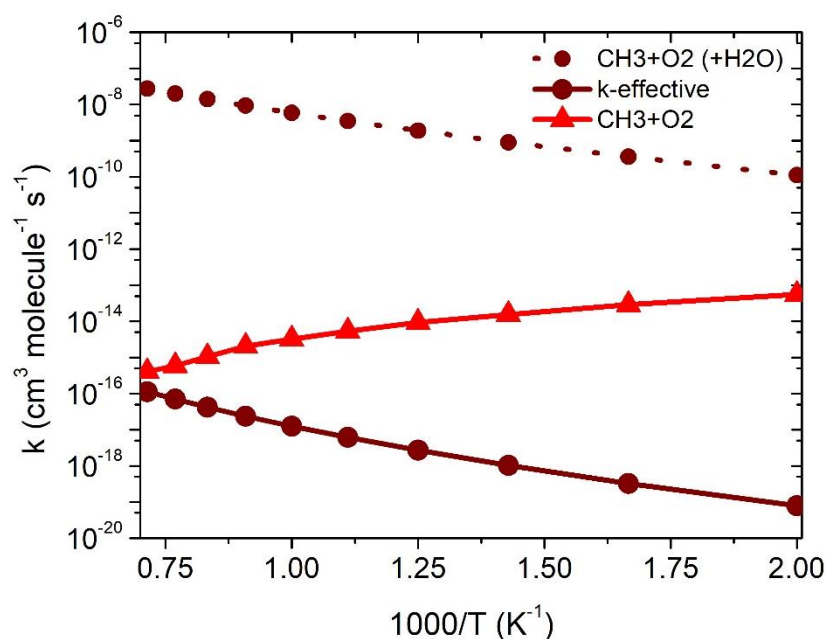


Figure 6. Rate constants for the effect of H₂O on $\bullet\text{CH}_3 + {}^3\text{O}_2$ reaction in the temperature range of 500–1500 K.

The total effective-rate constants were calculated using $k_h^{eff} = K_{eq(1h)} \times k(RRKM) \times [\text{H}_2\text{O}]$. Where $K_{eq(1h)}$ are the equilibrium constants of the $\bullet\text{CH}_3 + \text{O}_2 \rightarrow \text{RC}$ reactions and $[\text{H}_2\text{O}]$ is the water concentration, as discussed in earlier studies [21,25]. The effective rate constant ($7 \times 10^{-17} \text{ cm}^3 \text{ molecule}^{-1} \text{ s}^{-1}$ at 1000 K) is ~two-order magnitude lower than the $\bullet\text{CH}_3 + {}^3\text{O}_2$ reaction ($\sim 6 \times 10^{-15} \text{ cm}^3 \text{ molecule}^{-1} \text{ s}^{-1}$ at 1000 K). Our result is also consistent with the previously reported value for a similar combustion-reaction system, i.e., $\bullet\text{CH}_2\text{OH} + {}^3\text{O}_2$ [26]. The effective rate constant suggests that the catalytic effect may be pronounced at a high temperature >1500 K, and the catalytic effect of H₂O may be important under a combustion condition >1500 K.

Figure 7 shows the comparison of the rate constants in all three reaction systems, and the rate constant values are given in Table 2. The rate constants for $\text{CH}_3 + \text{O}_2$ are negative-temperature-dependent, however, the rate constants for the effect of CO₂ and H₂O are positive-temperature-dependent. These results are due to fact that the TSs and RCs of CO₂ and H₂O have different values of energies, entropic factors and concentrations. In general, the effective rate constants for the CO₂-assisted reactions are higher at >1400 K, while those for the H₂O-assisted reactions are almost similar at >1500 K to the $\bullet\text{CH}_3 + \text{O}_2$ -reaction system (Figure 7). The rate constant at 1000 K is at least one–two-order magnitude smaller than $\bullet\text{CH}_3 + \text{O}_2$. As a result, the effect of $\bullet\text{CH}_3 + \text{O}_2$ catalyzed by CO₂ and H₂O is of only minor importance for the sink of $\bullet\text{CH}_3$ in a gas-phase-combustion reaction. Such results are interesting. We believe the present results provide insights into a better understanding of the gas-phase catalytic effect of CO₂ and H₂O molecules on the most important combustion-prototype molecule.

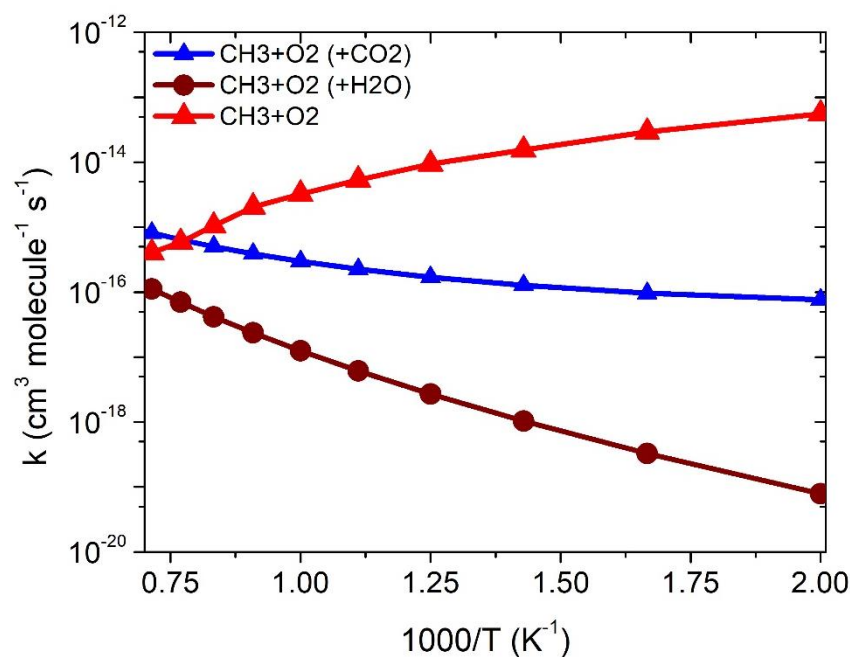


Figure 7. Comparison of the rate constants between $\bullet\text{CH}_3 + {}^3\text{O}_2$, $\bullet\text{CH}_3 + \text{O}_2 (+\text{CO}_2)$ and $\bullet\text{CH}_3 + \text{O}_2 (+\text{H}_2\text{O})$ reactions.

4. Conclusions

We have predicted the rate constants for the $\bullet\text{CH}_3 + {}^3\text{O}_2$ reaction, and the effect of CO_2 and H_2O molecules on the $\bullet\text{CH}_3 + {}^3\text{O}_2$ reaction using the CC-p/M06-p method, coupled with the RRKM/ME simulation, between a temperature range of 500 to 1500 K and a pressure range of 0.0001 to 10 atm. The results show that $\bullet\text{CH}_3 + {}^3\text{O}_2$ leads to form CH_2O and OH at a temperature > 1300 K, which is consistent with the previous studies. The calculated rate constants for $\bullet\text{CH}_3 + {}^3\text{O}_2$ are in good agreement with the previously measured experimental values. When CO_2 and H_2O molecules are introduced to the $\bullet\text{CH}_3 + {}^3\text{O}_2$ reaction, the reaction unfavored the formation of CH_2O below 1300 K. The calculated rate constants for the effect of CO_2 and H_2O are independent of pressure and show positive-temperature dependence. The result suggests that the effect of CO_2 and H_2O shows a non-RRKM behavior, and the $\text{CH}_3 + \text{O}_2$ reaction shows an RRKM behavior. This result is unique, and it was observed for the first time. Our results also demonstrate that single CO_2 and H_2O molecules have the potential to accelerate a gas-phase reaction at a higher temperature > 1300 K and slow the reaction at a lower temperature.

Under the combustion condition, the kinetics of $\bullet\text{CH}_3 + \text{O}_2 (+\text{CO}_2)$ are quite different from those of $\bullet\text{CH}_3 + \text{O}_2 (+\text{H}_2\text{O})$. This difference is possibly due to the reaction energies and concentrations of CO_2 and H_2O being different. These kinds of results are interesting, so experimental measurements are required to validate these findings. Based on current findings and previous findings, we can conclude that the main kinetic mechanism of $\bullet\text{CH}_3 + {}^3\text{O}_2 \rightarrow \text{CH}_2\text{O} + \text{HO}$ via $\bullet\text{CH}_3\text{OO}$ (Int-1) and other mechanisms, such as the formation of RC via a TS1 to Int-1, is almost negligible. Such a weakly bound complex RC should not be included in the kinetic calculations under the combustion condition. In the case of the effect of H_2O and CO_2 , the formations of RC-c and RC-h are important, and the catalytic effect has a negative effect under combustion conditions.

Supplementary Materials: The following supporting information can be downloaded at: <https://www.mdpi.com/article/10.3390/catal12070699/s1>. The optimized geometries of all the species involved in $\bullet\text{CH}_3 + {}^3\text{O}_2$, $\bullet\text{CH}_3 + {}^3\text{O}_2 (+\text{CO}_2)$, and $\bullet\text{CH}_3 + {}^3\text{O}_2 (+\text{H}_2\text{O})$ are given in Table S1. The rot-vib parameter for all the species is given in Table S2, and the equilibrium constants are given in Table S3. The details of the chemical kinetic calculations are given in the Supporting Information.

Author Contributions: M.R.D. completed all the Gaussian calculations; M.A.A. and L.M.A.M. completed the chemical kinetic calculations; M.A.A. and M.R.D. prepared the draft of the manuscript. All authors have read and agreed to the published version of the manuscript.

Funding: This research was funded by Deanship of Scientific Research, Vice Presidency for Graduate Studies and Scientific Research, King Faisal University, Saudi Arabia grant number [AN000532] and the APC was funded by Deanship of Scientific Research, Vice Presidency for Graduate Studies and Scientific Research, King Faisal University, Saudi Arabia grant number [AN000532].

Data Availability Statement: All the quantum chemical data generated through this study are given in the Supporting Information.

Acknowledgments: Mohamad Akbar Ali (M.A.A.) gratefully acknowledges the Annual Funding track by the Deanship of Scientific Research, Vice Presidency for Graduate Studies and Scientific Research, King Faisal University, Saudi Arabia [Project No. AN000532].

Conflicts of Interest: The authors declare no competing interests.

References

1. Srinivasan, N.K.; Su, M.-C.; Sutherland, J.W.; Michael, J.V. Reflected Shock Tube Studies of High-Temperature Rate Constants for $\text{OH} + \text{CH}_4 \rightarrow \text{CH}_3 + \text{H}_2\text{O}$ and $\text{CH}_3 + \text{NO}_2 \rightarrow \text{CH}_3\text{O} + \text{NO}$. *J. Phys. Chem. A* **2005**, *109*, 1857–1863. [[CrossRef](#)] [[PubMed](#)]
2. Vaghjiani, G.L.; Ravishankara, A.R. New measurement of the rate coefficient for the reaction of OH with methane. *Nature* **1991**, *350*, 406–409. [[CrossRef](#)]
3. Baulch, D.L.; Cobos, C.J.; Cox, R.A.; Esser, C.; Frank, P.; Just, T.; Kerr, J.A.; Pilling, M.J.; Troe, J.; Walker, R.W.; et al. Evaluated Kinetic Data for Combustion Modelling. *J. Phys. Chem. Ref. Data* **1992**, *21*, 411. [[CrossRef](#)]
4. Srinivasan, N.K.; Su, M.-C.; Michael, J.V. $\text{CH}_3 + \text{O}_2 \rightarrow \text{H}_2\text{CO} + \text{OH}$ Revisited. *J. Phys. Chem. A* **2007**, *111*, 11589–11591. [[CrossRef](#)] [[PubMed](#)]
5. Herbon, J.T.; Hanson, R.K.; Bowman, C.T.; Golden, D.M. The reaction of $\text{CH}_3 + \text{O}_2$: Experimental determination of the rate coefficients for the product channels at high temperatures. *Proc. Combust. Inst.* **2005**, *30*, 955–963. [[CrossRef](#)]
6. Hsu, D.S.Y.; Shaub, W.M.; Creamer, T.; Gutman, D.; Lin, M.C. Kinetic modeling of co-production from the reaction of CH_3 with O_2 in shock waves. *Ber. Bunsenges. Phys. Chem.* **1983**, *87*, 909–991. [[CrossRef](#)]
7. Cobos, C.J.; Hippler, H.; Luther, K.; Ravishankara, A.R.; Troe, J. High-pressure falloff curves and specific rate constants for the reaction $\text{CH}_3 + \text{O}_2 \leftrightarrow \text{CH}_3\text{O}_2 \leftrightarrow \text{CH}_3 + \text{O}$. *J. Phys. Chem.* **1985**, *89*, 4332–4338. [[CrossRef](#)]
8. Zhang, F.; Huang, C.; Xie, B.; Wu, X. Revisiting the chemical kinetics of $\text{CH}_3 + \text{O}_2$ and its impact on methane ignition. *Combust. Flame* **2019**, *200*, 125–134. [[CrossRef](#)]
9. Masunov, A.E.; Wait, E.; Vasu, S.S. Quantum Chemical Study of $\text{CH}_3 + \text{O}_2$ Combustion Reaction System: Catalytic Effects of Additional CO_2 Molecule. *J. Phys. Chem. A* **2017**, *121*, 5681–5689. [[CrossRef](#)]
10. Pilling, M.J.; Smith, M.J.C. A laser flash photolysis study of the reaction $\text{CH}_3 + \text{O}_2 \rightarrow \text{CH}_3\text{O}_2$ at 298 K. *J. Phys. Chem.* **1985**, *89*, 4713–4720. [[CrossRef](#)]
11. Zhu, R.; Hsu, C.-C.; Lin, M.C. Ab initio study of the $\text{CH}_3 + \text{O}_2$ reaction: Kinetics, mechanism and product branching probabilities. *J. Chem. Phys.* **2011**, *115*, 195. [[CrossRef](#)]
12. Tan, Y.; Douglas, M.A.; Thambimuthu, K.V. CO_2 Capture Using Oxygen Enhanced Combustion Strategies for Natural Gas Power Plants. *Fuel* **2002**, *81*, 1007–1016. [[CrossRef](#)]
13. Kumar, A.; Mallick, S.; Mishra, B.M.; Kumar, P. Effect of ammonia and formic acid on the $\text{CH}_3\text{O} + \text{O}_2$ reaction: A quantum chemical investigation. *Phys. Chem. Chem. Phys.* **2020**, *22*, 2405–2413. [[CrossRef](#)] [[PubMed](#)]
14. Wu, C.H.; Lin, C.Y.; Wang, H.T.; Lin, M.C. A shock tube study of the oxidation of the methyl radical. *AIP Conf. Proc.* **1990**, *208*, 450–455.
15. Zhang, T.; Zhang, Y.; Wen, M.; Tang, Z.; Long, B.; Yu, X.; Zhao, C.; Wang, W. Effects of water, ammonia and formic acid on $\text{HO}_2 + \text{Cl}$ reactions under atmospheric conditions: Competition between a stepwise route and one elementary step. *RSC Adv.* **2019**, *9*, 21544–21556. [[CrossRef](#)]
16. Srinivasan, N.K.; Su, M.C.; Sutherland, J.W.; Michael, J.V. Reflected shock tube studies of high-temperature rate constants for $\text{CH}_3 + \text{O}_2$, $\text{H}_2\text{CO} + \text{O}_2$, and $\text{OH} + \text{O}_2$. *J. Phys. Chem. A* **2005**, *109*, 7902–7914. [[CrossRef](#)]
17. Masunov, A.E.; Elizabeth, E.; Wait, S.; Vasu, S. Catalytic Effect of Carbon Dioxide on Reaction $\text{OH} + \text{CO} \rightarrow \text{H} + \text{CO}_2$, in Supercritical Environment: Master Equation Study. *J. Phys. Chem. A* **2018**, *122*, 6355–6359. [[CrossRef](#)]
18. Pryor, O.M.; Barak, S.; Koroglu, B.; Ninnemann, E.; Vasu, S.S. Measurements and Interpretation of Shock Tube Ignition Delay Times in Highly CO_2 Diluted Mixtures Using Multiple Diagnostics. *Combust. Flame* **2017**, *180*, 63–76. [[CrossRef](#)]
19. Koroglu, B.; Pryor, O.; Lopez, J.; Nash, L.; Vasu, S.S. Shock Tube Ignition Delay Times and Methane Time-Histories Measurements During Excess CO_2 Diluted Oxy-Methane Combustion. *Combust. Flame* **2016**, *164*, 152–163. [[CrossRef](#)]
20. Zhang, W.; Du, B.; Qin, Z. Catalytic effect of Water, Formic Acid, or Sulfuric Acid on the Reaction of Formaldehyde with OH Radicals. *J. Phys. Chem. A* **2014**, *118*, 4797–4807. [[CrossRef](#)]

21. Jara-Toro, R.A.; Hernández, F.J.; Taccone, R.A.; Lane, S.I.; Pino, G.A. Water catalysis of the reaction between methanol and OH at 294 K and the atmospheric implications. *Angew. Chem. Int. Ed.* **2017**, *56*, 2166–2170. [[CrossRef](#)] [[PubMed](#)]
22. Wu, J.; Gao, L.G.; Varga, Z.; Xu, X.; Ren, W.; Truhlar, D.G. Water catalysis of the Reaction of Methanol with OH Radical in the Atmosphere is Negligible. *Angew. Chem. Int. Ed.* **2020**, *59*, 10826–10830. [[CrossRef](#)] [[PubMed](#)]
23. Vöhringer-Martinez, E.; Hansmann, B.; Hernandez, H.; Francisco, J.S.; Troe, J.; Abel, B. Water Catalysis of a Radical-Molecule Gas-Phase Reaction. *Science* **2007**, *315*, 496–501. [[CrossRef](#)]
24. Thomsen, D.; Kurtén, T.; Jørgensen, S.; Wallington, T.; Baggesen, S.; Aalling, C.; Kjaergaard, H. On the possible catalysis by single water molecules of gas-phase hydrogen abstraction reactions by OH radicals. *Phys. Chem. Chem. Phys.* **2012**, *14*, 12992–12999. [[CrossRef](#)] [[PubMed](#)]
25. Chao, W.; Lin, J.J.; Takahashi, K.; Tomas, A.; Yu, L.; Kajii, Y.; Batut, S.; Schoemaeker, C.; Fittschen, C. Water vapor does not catalyze the reaction between methanol and OH Radicals. *Angew. Chem. Int. Ed.* **2019**, *58*, 5013–5017. [[CrossRef](#)]
26. Dash, M.R.; Ali, M.A. Effect of a single water molecule on $\text{CH}_2\text{OH} + {}^3\text{O}_2$ reaction under atmospheric and combustion conditions. *Phys. Chem. Chem. Phys.* **2022**, *24*, 1510–1519. [[CrossRef](#)] [[PubMed](#)]
27. Ali, M.A.; Balaganesh, M.; Lin, K.C. Catalytic effect of a single water molecule on the OH + CH_2NH reaction. *Phys. Chem. Chem. Phys.* **2018**, *20*, 4297–4307.
28. Ali, M.A.; Ali, M.A. Effect of Water and Formic Acid on $\cdot\text{OH} + \text{CH}_4$ Reaction: An Ab Initio/DFT Study. *Catalysts* **2022**, *12*, 133. [[CrossRef](#)]
29. Inaba, S. Catalytic Role of H_2O Molecules in Oxidation of CH_3OH in Water. *Catalysts* **2018**, *8*, 157. [[CrossRef](#)]
30. Ali, M.A.; Balaganesh, M.; Jang, S. Can a single water molecule catalyze the OH+ CH_2CH_2 and OH+ CH_2O reactions? *Atmos. Environ.* **2019**, *207*, 82–92. [[CrossRef](#)]
31. Ali, M.A.; Balaganesh, M.; Al-Odail, F.A.; Lin, K.C. Effect of ammonia and water molecule on OH + CH_3OH reaction under tropospheric condition. *Sci. Rep.* **2021**, *11*, 12185. [[CrossRef](#)] [[PubMed](#)]
32. Ali, M.A. Computational studies on the gas phase reaction of methylenimine (CH_2NH) with water molecules. *Sci. Rep.* **2020**, *10*, 10995. [[CrossRef](#)] [[PubMed](#)]
33. Buszek, R.J.; Torrent-Sucarrat, M.; Anglada, J.M.; Francisco, J.S. Effects of a Single Water Molecule on the OH + H_2O_2 Reaction. *J. Phys. Chem. A* **2012**, *116*, 5821–5829. [[CrossRef](#)]
34. Iuga, C.; Alvarez-Idaboy, J.R. On the Possible Catalytic Role of a Single Water Molecule in the Acetone + OH Gas Phase reaction: A Theoretical Pseudo-Second-order Kinetics Study. *Theor. Chem. Acc.* **2011**, *129*, 209–217. [[CrossRef](#)]
35. Iuga, C.; Alvarez-Idaboy, J.R.; Reyes, L.; Vivier-Bunge, A. Can a Single Water Molecule Really Catalyze the Acetaldehyde OH Reaction in Tropospheric Conditions? *J. Phys. Chem. Lett.* **2010**, *1*, 3112–3115. [[CrossRef](#)]
36. Zhang, T.; Wang, W.; Li, C.; Du, Y.; Lu, J. Catalytic effect of a single water molecule on the atmospheric reaction of $\text{HO}_2 + \text{OH}$: Fact or fiction? A mechanistic and kinetic study. *RSC Adv.* **2013**, *3*, 7381–7391. [[CrossRef](#)]
37. Frisch, M.J.; Trucks, G.W.; Schlegel, H.B.; Scuseria, G.E.; Robb, M.A.; Cheeseman, J.R.; Montgomery, T., Jr.; Vreven, K.N.; Kudin, J.C.; Burant, J.M.; et al. *Gaussian 09, Revision D.01*; Gaussian, Inc.: Wallingford, CT, USA, 2013.
38. Zhao, Y.; Truhlar, D.G. The M06 Suite of Density Functionals for Main Group Thermochemistry, Thermochemical Kinetics, Noncovalent Interactions, Excited States, and Transition Elements: Two New Functionals and Systematic Testing of Four M06-Class Functionals and 12 other Functionals. *Theor. Chem. Acc.* **2008**, *120*, 215–241.
39. Barker, J.R.; Nguyen, T.L.; Stanton, J.F.; Aieta, C.; Ceotto, M.; Gabas, F.; Kumar, T.J.D.; Li, C.G.L.; Lohr, L.L.; Maranzana, A.; et al. *MultiWell-<Version>-Software Suite*; Barker, J.R., Ed.; University of Michigan: Ann Arbor, MI, USA, 2016. Available online: <https://multiwell.engin.umich> (accessed on 24 May 2022).
40. Ruscic, B.; Pinzon, R.E.; Morton, M.L.; von Laszewski, G.; Bittner, S.J.; Nijssure, S.G.; Amin, K.A.; Minkoff, M.; Wagner, A.F. Introduction to Active Thermochemical Tables: Several “Key” Enthalpies of Formation Revisited. *J. Phys. Chem.* **2004**, *108*, 9979–9997. [[CrossRef](#)]
41. Ruscic, B.; Pinzon, R.E.; Von Laszewski, G.; Kodeboyina, D.; Burcat, A.; Leahy, D.; Montoy, D.; Wagner, A.F. Active Thermochemical Tables: Thermochemistry for the 21st Century. *J. Phys. Conf. Ser.* **2005**, *16*, 561–570. [[CrossRef](#)]
42. Ruscic, B.; Bross, D.H. Active Thermochemical Tables (ATcT) Enthalpies of Formation Values Based on ver. 1.112r of the Thermochemical Network. 2021. Available online: [ATcT.anl.gov](https://atct.anl.gov) (accessed on 24 May 2022).
43. Lemmon, E.W.; McLinden, M.O.; Friend, D.G. Thermophysical Properties of Fluid Systems. In *NIST Chemistry Webbook*; NIST Standard Reference Database Number 69. Available online: <https://atct.anl.gov/> (accessed on 24 May 2022).
44. Metcalfe, W.K.; Burke, M.; Ahmed, S.S.; Curran, H.J. A Hierarchical and Comparative Kinetic Modeling Study of C1–C2 Hydrocarbon and Oxygenated Fuels. *Int. J. Chem. Kinet.* **2013**, *45*, 638–675. [[CrossRef](#)]